Journal of Molecular Liquids 198 (2014) 107–113

Contents lists available at ScienceDirect

Journal of Molecular Liquids

journal homepage: www.elsevier.com/locate/molliq

Molecular dynamics simulations of water on a hydrophilic silica surface at high air pressures

H.A. Zambrano [a], J.H. Walther [b,c,*], R.L. Jaffe [d]

[a] Department of Chemical Eng., Universidad de Concepcion, Concepcion, Chile
[b] Department of Mechanical Engineering, Technical University of Denmark, DK-2800 Lyngby, Denmark
[c] Chair of Computational Science, ETH Zürich, Universitätsstrasse 6, CH-8092 Zürich, Switzerland
[d] NASA Ames Research Center, Moffett Field, CA 94035, USA

ARTICLE INFO

Article history:
Received 11 February 2012
Received in revised form 22 April 2014
Accepted 2 June 2014
Available online 14 June 2014

Keywords:
Molecular dynamics
Wetting
Nanodroplets
Contact angle
Solid–liquid–gas interactions

ABSTRACT

We present a force field for Molecular Dynamics (MD) simulations of water and air in contact with an amorphous silica surface. We calibrate the interactions of each species present in the system using dedicated criteria such as the contact angle of a water droplet on a silica surface, and the solubility of air in water at different pressures. Using the calibrated force field, we conduct MD simulations to study the interface between a hydrophilic silica substrate and water surrounded by air at different pressures. We find that the static water contact angle is independent of the air pressure imposed on the system. Our simulations reveal the presence of a nanometer thick layer of gas at the water–silica interface. We believe that this gas layer could promote nucleation and stabilization of surface nanobubbles at amorphous silica surfaces.

1. Introduction

The static and dynamic properties of fluids at solid surfaces have been the subject of intense research during the last decades [1–7]. Wetting phenomena have been studied extensively [8–10], but several questions relating to interfacial *dynamic* properties remain open due to theoretical, experimental and computational limitations. Wetting is essential and ubiquitous in a variety of natural and technological processes [11–15]. Miniaturization, a trend in several technological fields, is leading to complex structures on the nanoscale [11,15,16]. Hence, the development of novel nanofluidic devices will require a comprehensive understanding of dynamic wetting phenomena at the nanoscale.

Silicon dioxide–water systems interacting with air are abundant in nature and play fundamental roles in a diversity of novel science and engineering applications such as silicon based nanosensor devices, nanoscale lab-on-a-chip systems and DNA microarray technologies [11,17–20]. Although extensive experimental, theoretical and computational work has been devoted to study the nature of the interaction between silica and water [7,13,21–29], many fundamental questions are currently subject of intense debate. Recently, in a number of experimental investigations, systematic deviations in the filling rate from classical predictions have been measured for silica channels with sub-nanometer size [30–35]. Thamdrup et al. [32] attributed the measured deviations to the presence of gas nanobubbles. In addition, the existence of nanoscale gas bubbles at solid–liquid interfaces has been proposed as an explanation for the long range hydrophobic forces measured in surface force apparatus experiments [2,36,37]. Nanobubbles have been observed and inferred in a variety of experimental and theoretical works on hydrophobic [1,37–47] and hydrophilic surfaces [1,47,48]. Nevertheless, the long lifetime of interfacial nanobubbles contradicts the classical theory of nanoscale bubble stability as their large Laplace pressure should cause a rapid diffusive out-flux of gas [49,50] leading to a rapid collapse of the bubble. However, in recent theoretical and experimental studies some potential stabilization mechanisms have been suggested to explain the observations of long lived nanobubbles [42,45,51–56]. Furthermore, in a recent experimental work, evidence of slippage has been found in hydrophilic nanochannels filled with water [57], which could suggest that an air layer could be present at the solid–water interface.

In this work we parameterize and calibrate an "effective" interaction potential in order to conduct long-timescale Molecular Dynamics (MD) simulations of systems including silica, water and air. Specifically, we study the role of air on the wetting of the water–silica interface.

2. Methodology and force fields

We conduct long MD simulations of hydrophilic silica–water–air systems using the MD package FASTTUBE [58]. FASTTUBE has been used extensively to study water inside and surrounding carbon

* Corresponding author at: Department of Mechanical Engineering, Technical University of Denmark, DK-2800 Lyngby, Denmark.
E-mail addresses: jhw@mek.dtu.dk, walther@mavt.ethz.ch (J.H. Walther).

http://dx.doi.org/10.1016/j.molliq.2014.06.003
0167-7322/

nanotubes, and in nano devices [59–65]. Since the objective of this work is the study of nanofluidic interfacial phenomena, the proposed silica–water–air model should allow efficient MD simulations of large systems for nanosecond timescales and be sufficiently reliable to reproduce the relevant effects related to the wetting properties of nanoscale systems. We use well tested models [66,67] for the species present in the system of interest and carry out a process of parameterization and calibration using dedicated criteria for each pairwise interaction [68]. The specific criteria used to calibrate the models are relevant to the properties we seek to reproduce.

2.1. Silica interaction potential

In the present study we model amorphous silica using the TTAMm potential developed by Guissani and Guillot [69], which is a modification of the TTAM model originally developed by Tsuneyuki et al. [66]. The TTAMm model includes Coulomb, Lennard–Jones (LJ) 6-18, and Buckingham potentials

$$\phi_{ab}\left(r_{ij}\right) = \frac{q_a q_b}{4\pi\varepsilon_0 r_{ij}^2} + \alpha_{ab}\exp\left(\frac{-r_{ij}}{\rho_{ab}}\right) - \frac{C_{ab}}{r_{ij}^6} + 4\epsilon_{ab}\left[\left(\frac{\sigma_{ab}}{r_{ij}}\right)^{18} - \left(\frac{\sigma_{ab}}{r_{ij}}\right)^{6}\right], \quad (1)$$

where q_a and q_b represent the partial charges of the atomic species a and b, ε_0 is the vacuum permittivity, r_{ij} the inter-atomic distance, σ_{ab} and ϵ_{ab} are the LJ parameters, and α_{ab}, ρ_{ab} and C_{ab} represent the Buckingham force field parameters. An overview of the potential parameters is presented in Table 1, where the subscripts *Si* and *Os* represent, respectively, silicon and oxygen atoms in silica. To describe the electrostatic interactions in the bulk silica system we employ partial charges obtained from the TTAM model [66]: $q_{Si} = +2.4e$ and $q_{Os} = -1.2e$. In order to construct an amorphous silica surface, we replicate a crystoballite cell to build a slab and carry out MD simulations imposing periodic boundary conditions in the x and y-directions, while imposing non-periodic boundary conditions in the z-direction in order to create a free surface. We use an integrating time step of 1 fs and follow a similar annealing procedure as employed by Huff et al. [70] and Cruz-Chu et al. [29]. Thus, we couple the system to a Berendsen heat bath [71], heating the crystoballite slab to 3000 K during 10 ps, followed by a subsequent quenching of the system from 3000 K to 300 K using a cooling rate of 70 K ps^{-1} until the equilibrium state is reached. Once silica is equilibrated, we classify the atoms at the surface of the silica slab according to their connectivity. Hence, a pair of atoms separated for a distance shorter than 0.2 nm is considered as covalently bonded. Silicon atoms with less than four covalent bonds and oxygen atoms with less than two covalent bonds are considered as dangling atoms. We compute a concentration of dangling oxygens of 1.50 atoms per nm^2 and a concentration of dangling silicons of 1.05 atoms per nm^2 which is in reasonable agreement with the calculations by Cruz-Chu et al. [29].

Table 1
Lennard–Jones, Buckingham parameters and partial charges for the TTAMm model [69].

Parameter	Value
ϵ_{Si-Si}	1.277×10^3 kJ mol^{-1}
σ_{Si-Si}	4.00×10^{-2} nm
ϵ_{Os-Os}	4.60×10^{-2} kJ mol^{-1}
σ_{Os-Os}	0.220 nm
ϵ_{Si-Os}	1.083 kJ mol^{-1}
σ_{Si-Os}	0.130 nm
α_{Si-Si}	8.417×10^{10} kJ mol^{-1}
ρ_{Si-Si}	1.522×10^2 nm
C_{Si-Si}	2.240×10^{-3} kJ mol^{-1} nm^6
α_{Os-Os}	1.696×10^5 kJ mol^{-1}
ρ_{Os-Os}	0.283×10^2 nm
C_{Os-Os}	0.0207 kJ mol^{-1} nm^6
α_{Si-Os}	1.0347×10^6 kJ mol^{-1}
ρ_{Si-Os}	0.480×10^2 nm
C_{Si-Os}	6.82510^{-3} kJ mol^{-1} nm^6
q_{Si}	$2.400e$
q_{Os}	$-1.200e$

2.2. Water interaction potential

Water is described using a modified version [72] of the rigid SPC/E model [67]. In this modified SPC/E model, Coulomb and van der Waals interactions are truncated at 1 nm, the electrostatic potential acting between the partial charges on the oxygen ($q_{Ow} = -0.8476e$), and hydrogen ($q_{Hw} = +0.4238e$) atoms is smoothed at the cut-off distance to guarantee energy conservation [58,59], while the van der Waals interactions described by using a Lennard–Jones 12-6 potential are truncated without smoothing

$$U_{ab}\left(r_{ij}\right) = 4\varepsilon_{ab}\left[\left(\frac{\sigma_{ab}}{r_{ij}}\right)^{12} - \left(\frac{\sigma_{ab}}{r_{ij}}\right)^{6}\right]. \quad (2)$$

The potential parameters for the SPC/E water model are listed in Table 2. It should be noted that in previous works, the truncated Coulomb potential with a proper smoothing has been used with success cf. [61,73–77]. Moreover, Zambrano et al. [78] conducted non-equilibrium MD simulations of a water-chloride solution on an amorphous silica substrate; the water interactions were described using the same modified SPC/E model but varying the cut-off distances to check the sensitivity of the model to the implemented truncation radius. Consistent water density profiles were obtained for cut-off distances exceeding 1.0 nm cf. [78].

Lastly, recent uncertainty quantification studies of MD simulations of water-graphitic systems [79] highlight that truncation should be viewed as an integral part of the MD potential and that large truncation radii or Ewald summation techniques do not guarantee more accurate predictions.

The SHAKE algorithm [80] is used in these simulations to keep the O – H distance fixed at 1 Å and the H – O – H angle at 109.47°.

2.3. Air interaction potential

We describe the air by modeling the molecular nitrogen and molecular oxygen as two Lennard–Jones sites connected with a rigid bond of length $r_{N-N} = 0.1094$ nm and $r_{O-O} = 0.1208$ nm cf. Jiang et al. [81]. The LJ parameters are listed in Table 3.

2.4. Silica–water interaction potential

Since long simulation times (ten to hundreds of nanoseconds) are required to study nanofluidic systems, our objective is to derive interaction potential models to be both highly efficient in terms of processing time and sufficient accurate to reproduce reliably the macroscale properties of the silica–water interface. In a previous work, Hassanali and Singer [25] developed a model which is an extension of the van Beest, Kramer, and van Santen (BKS) model [82] for silica and of the SPC/E

Table 2
Lennard–Jones parameters and partial charges for the SPC/E water model [67].

Parameter	Value
ϵ_{Ow-Ow}	0.6501 kJ mol^{-1}
σ_{Ow-Ow}	0.3166 nm
q_{Ow}	$-0.8476e$
q_{Hw}	$0.4238e$

Table 3
Lennard–Jones interaction parameters for the air model [81].

Parameters	Value
ϵ_{N-N}	0.3026 kJ mol^{-1}
σ_{N-N}	0.3320 nm
ϵ_{O-O}	0.4323 kJ mol^{-1}
σ_{O-O}	0.2990 nm
ϵ_{N-O}	0.3617 kJ mol^{-1}
σ_{N-O}	0.3155 nm

model [67] for water. They added three body interaction terms which are not found in the standard BKS model and obtained the potential parameters from ab initio quantum chemical studies on small fragments of silica–water systems. In the present study we retain the simple and efficient two body Born–Huggins–Mayer potential, which consists of Coulomb potential and Buckingham potential terms

$$\mu_{ab}\left(r_{ij}\right) = \frac{q_a q_b}{4\pi\varepsilon_0 r_{ij}^2} + \alpha_{ab}\exp\left(\frac{-r_{ij}}{\rho_{ab}}\right) - \frac{C_{ab}}{r_{ij}^6}. \quad (3)$$

We equilibrate the silica slab as described in Section 2.1. The water is immobilized during the amorphous silica equilibration and cooling process. Due to the fact that, for amorphous silica, the surficial electrostatics are significantly different from the bulk electrostatics, we modify the partial charges of the rigid silica model following a similar procedure to that employed by Cruz-Chu et al. [29]. However we modify the value of the partial charge for all atoms in the slab rather than defining a subset of atoms as surface atoms. The partial charge values are taken from the soft potential developed by Takada et al. [83], which has electrostatic interactions weaker than the partial charges used in classical silica models, thus: $q_{Os} = -0.65e$ for the oxygen atoms and $q_{Si} = 1.3e$ for the silicon atoms. It should be noted that the silica slab is electrically neutral since the new values of the silicon and oxygen partial charge keep the same proportion as the charges in the original TTAM [66]. Subsequently, we equilibrate the water, immobilizing the silica and coupling the water to a Berendsen thermostat until the energy of the system has reached a constant value. We perform simulations of a water droplet of 18,000 molecules placed on a silica substrate of 37.92 nm × 37.92 nm × 2.4 nm (ca. 350000 atoms) as shown in Fig. 1. For the simulations we use an integrating time steps of 2 fs.

Note that an important difference relative to the models previously developed by Cruz-Chu et al. [29] and Hassanali and Singer [25] is that we do not include silanol groups on the silica surface. Here, we attempt to capture the effective wetting of the silica surface by calibrating the Buckingham potential to describe the silica–water interaction. In fact, in this work we use the water contact angle as criterion to calibrate our potentials thus the size of the silica–water system is important in order to take into account the effect of the heterogeneities present in the amorphous silica surface on the wetting of the system without explicitly including silanols. Thus, to achieve a suitable force field for the silica–water interaction we adjust the Buckingham parameter C_{Si-Ow} to match the experimental water contact angle (WCA: θ) of 19.9° cf. [32,33]. The WCA is determined following the procedure employed by Werder et al. [84] but we do not a priori assume a spherical droplet therefore performing a local fit of the cross section similar to Ingebrigtsen and Toxvaerd [85]. We vary systematically the value of C_{Si-Ow} from 0 kJ mol^{-1} nm^6, the value proposed by Hassanali and Singer [25], to 0.03 kJ mol^{-1} nm^6 in increments of 0.005 kJ mol^{-1} nm^6. We find that $C_{Si-Ow} = 0$ kJ mol^{-1} nm^6 produces a strongly hydrophobic interface with a WCA of $\theta = 97°$, whereas $C_{Si-Ow} = 0.03$ kJ mol^{-1} nm^6 results in complete wetting ($\theta = 0°$) cf. Fig. 2. Within this range of parameters we furthermore find that the WCA varies linearly in C_{Si-Ow}, as

$$\theta = 104^{\circ} - 3560^{\circ}\left(\text{kJ mol}^{-1}\ \text{nm}^6\right)^{-1} C_{Si-Ow}, \quad (4)$$

and matches the experimental WCA of 19.9° [32] with $C_{Osi-Ow} = 2.360 \times 10^{-2}$ kJ mol^{-1} nm^6. The potential parameters are summarized in Table 4. To quantify the strength of the water–silica interaction, we measure the binding energy of a single water molecule on the amorphous silica surface. We find a mean binding energy of 45 kJ mol^{-1} which is in reasonable agreement with the results published by Du et al. [86] which vary between 48 kJ mol^{-1} to 98 kJ mol^{-1} for a water molecule on H-terminated and pure silica clusters.

2.5. Silica–air interaction potential

The interactions between silica and the sites of the molecular nitrogen and molecular oxygen are described employing a LJ potential using Lorentz–Berthelot mixing rules with values obtained from the Universal Force Field (UFF) [87] and from Guissani and Guillot [69]. The parameters are shown in Table 5. To examine the reliability of the potential we conduct MD simulations of a silica slab surrounded by an air atmosphere at different air pressures. We equilibrate a silica slab as described in Section 2.1. Subsequently, we perform simulations of the equilibrated silica slab surrounded by air at 100 bar and 200 bar for more than 4 ns. From the simulations we extract the density profiles of nitrogen and oxygen. We observe an air interfacial layer with a

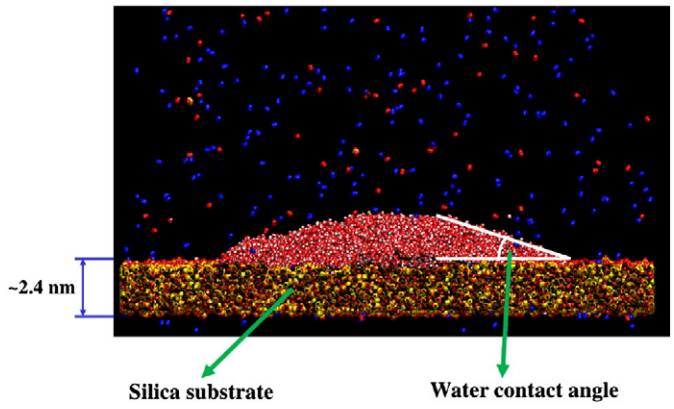

Fig. 1. Contact angle of a water nanodroplet on an amorphous silica slab. Snapshot from a MD simulation of a water nano-droplet mounted on a silica slab subject to a high air pressure (10 bar).

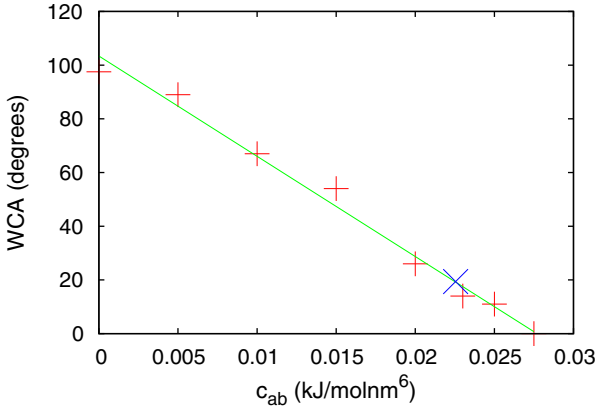

Fig. 2. Water contact angle (WCA) of a water nanodroplet on a silica surface as a function of the Buckingham interaction parameter C_{ab}. Red (+): WCA determined in vacuum; blue (×): the value fitted to the experimental WCA; green (—) linear fit to the computed data.

Table 4
Buckingham parameters for the silica–water interaction potential.

Parameter	Value
α_{Si-Ow}	1.013×10^5 kJ mol^{-1}
ρ_{Si-Ow}	25.00 nm
C_{Si-Ow}	2.360×10^{-2} kJ mol^{-1} nm^6
α_{Osi-Hw}	6.83×10^3 kJ mol^{-1}
ρ_{Osi-Hw}	32.66 nm
C_{Osi-Hw}	0 kJ mol^{-1} nm^6

thickness of ca. 1 nm as shown in Fig. 3. In this zone the air density is higher than the air density in the bulk zone. It should be noted that in a molecular description of an interface, the position of a solid surface is somewhat arbitrary since the atoms are fuzzy. In this study the approach suggested by Travis and Gubbins [88] was followed. Thus, the wall is assumed to be placed one atomic diameter from the wall atoms.

To provide validation for the silica–air interaction, we conduct molecular dynamics simulations of single molecules of N_2 and O_2 on a silica substrate. We measure the binding energy of the molecules of N_2 and O_2 on the silica surface. We obtain a binding energy of 22 kJ mol^{-1} for the N_2 molecule and of 18 kJ mol^{-1} for the O_2 molecule. Furthermore, we perform simulations of a nitrogen molecule described using the "pea model" developed by Coasne et al. [89] on a silica slab. We measure a binding energy of 13.5 kJ mol^{-1} which is in reasonable agreement with the present results.

2.6. Water–air interaction potential

The interaction between water and air is simulated employing a Lennard–Jones 12-6 potential (Eq. (2)), which is initially parameterized using Lorentz–Berthelot mixing rules. The values for the mixing rules are obtained from Jiang et al. [81] cf. Table 3 and the values from the SPC/E water model cf. Table 2. Thus, the initial values are: $\epsilon_{N-Ow} = 0.4436$ kJ mol^{-1}, $\sigma_{N-Ow} = 0.3243$ nm, $\epsilon_{O-Ow} = 0.5302$ kJ mol^{-1}, and $\sigma_{O-Ow} = 0.3078$ nm. To obtain a suitable potential for the interaction between water and air we calibrate the LJ potential parameters ϵ_{N-Ow} and ϵ_{O-Ow} using as a criterion the gas solubility in liquid water. We perform simulations of a water slab including 2800 molecules immersed in an atmosphere of N_2 and O_2 at different pressures. We connect the system to a Berendsen thermostat for 0.4 ns at 300 K, then we disconnect the thermostat and perform simulations for more than 30 ns until the water slab is saturated with air. We measure the density of nitrogen and oxygen dissolved in water and compute the solubility of the two species. We compare the gas solubility values extracted from the simulations against the experimental values [90,91] listed in Table 6. We calibrate the Lennard–Jones parameters by systematically varying the ϵ_{N-Ow} and ϵ_{O-Ow} values using as criteria the corresponding gas solubility values extracted from the simulations. We find that the solubility (s) varies linearly with ϵ_{N-Ow} and ϵ_{O-Ow} cf. Fig. 4

$$s_N = -8.1 + 18.9\epsilon_{N_0w}, \tag{5}$$

Table 5
Lennard–Jones parameters for air–silica interactions.

Parameters	Value
ϵ_{N-Si}	0.7963 kJ mol^{-1}
σ_{N-Si}	0.325 nm
ϵ_{N-Osi}	0.3075 kJ mol^{-1}
σ_{N-Osi}	0.293 nm
ϵ_{O-Si}	0.650 kJ mol^{-1}
σ_{O-Si}	0.318 nm
ϵ_{O-Osi}	0.251 kJ mol^{-1}
σ_{O-Osi}	0.290 nm

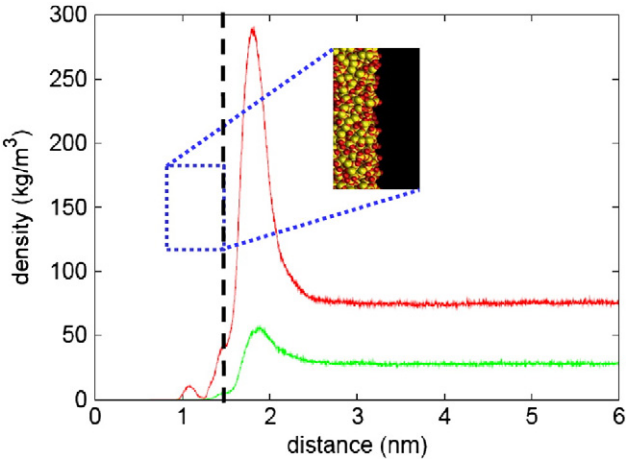

Fig. 3. Density profile of air at a silica surface at 300 K and 100 bar. The red line shows the N_2 density profile; and the green line the O_2 density profile. In this plot, the silica surface atoms are placed at ca. 1.5 nm.

$$s_O = -35.8 + 68.7\epsilon_{O_0w}, \tag{6}$$

and obtain the calibrated values through interpolation, with $\epsilon_{N-Ow} = 0.5458$ kJ mol^{-1} and $\epsilon_{O-Ow} = 0.5884$ kJ mol^{-1} cf. Table. 7. We perform simulations using the calibrated potential parameters and compute the gas solubility. The density profiles of nitrogen and oxygen throughout the water slab are shown in Fig. 5. The gas solubility values computed from the density values extracted from the simulations cf. Table 8 are found to reproduce (within 30%) the solubility to which they were fitted (Table 6). Although, simulations have been conducted for more than 30 ns, in Fig. 5B it is noted that oxygen solubility profiles are still not fully converged, however longer simulations are beyond our capabilities.

3. Results and discussion

3.1. Water contact angle of water nanodroplets on a silica surface at different air pressures

Using the parameterized and calibrated potentials we perform simulations of a water nanodroplet consisting of 18000 molecules mounted on a silica slab of 37.92 nm × 37.92 nm × 2.4 nm in vacuum and immersed in air (N_2 and O_2) at 50 bar, 100 bar, and 150 bar. To equilibrate the silica and the water we follow the methodology described in Section 2.4 while the air is immobilized. As silica–water equilibration is reached we release the air molecules to interact with the rest of the species until the system is equilibrated. We subsequently measure the WCA following the methodology described in Section 2.4. The resulting WCAs shown in Table 9 indicate that the static WCA of the nanodroplet is insensitive to the presence of air.

Table 6
Experimental values of the solubilities of nitrogen and oxygen in liquid water [90,91]. The solubility values included in the list have been interpolated at 300 K.

Specie	Pressure	Solubility
N_2	100 bar	1.265 cm^3_{gas}/g_{H_2O}
O_2	100 bar	2.417 cm^3_{gas}/g_{H_2O}
N_2	200 bar	2.257 cm^3_{gas}/g_{H_2O}
O_2	200 bar	4.621 cm^3_{gas}/g_{H_2O}

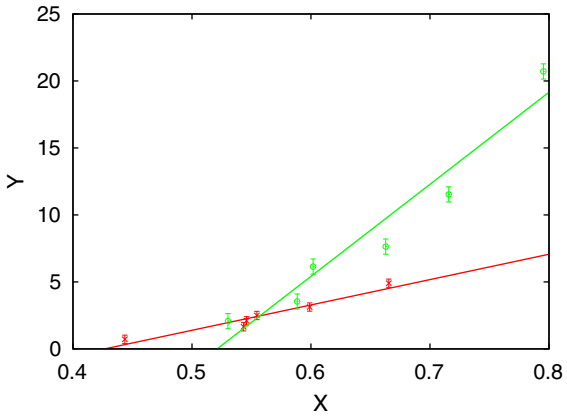

Fig. 4. The oxygen and nitrogen solubilities at 300 K and 200 bar as a function of the Lennard–Jones parameters ϵ_{N-Ow} and ϵ_{O-Ow}. ∘: (green) corresponds to ϵ_{O-Ow} values, and ×: (red) corresponds to ϵ_{N-Ow} values.

3.2. High density air layers at the silica–water interface

To study the energetics of the silica–water–air system, we perform simulations using the parameterized force field of a system consisting of a water slab (2800 molecules) on a silica substrate of 3.7 nm × 33.7 nm × 2.4 nm surrounded by an atmosphere of air at pressures of 50 bar, 100 bar, 200 bar, and 300 bar. In order to equilibrate the system we follow the methodology described in Sections 2.4 and 3.1. After water is saturated with air, which takes more than 30 ns, we measure the density of water, nitrogen and oxygen as a function of the distance to the silica slab. Moreover, we compute the solubility of nitrogen and oxygen dissolved in the water from the corresponding density values. Density profiles are shown in Fig. 6. From our simulations we observe a layer of high concentration of air adjacent to the silica surface, with a thickness of ca. 1 nm cf. Fig. 6. Moreover, we observe that the thickness and density of the layer are insensitive to the air pressure imposed to the system. Since this interfacial zone with a high gas concentration is present in all of our measurements we believe that it could be ever present in silica–water–air systems. Moreover, this layer could be of significant importance in dewetting, nucleation and stability of surficial nanobubbles, and capillary filling of silica nanochannels. Furthermore, the air layer inferred in this study could be related to the slippage reported in a recent experimental work [57].

We compute the binding energy of silica–water in vacuum and in the presence of air at very high pressures as illustrated in Table 10. We find that the values of the binding energy do not show a significant variation due to the presence of air in water. However, the interfacial layer with high concentration of gas may influence the dynamics of the interface e.g. through a modified viscosity [92] at the interface of silica and water. Recent experiments of capillary filling process of silica nanochannels have shown that the liquid is observed to fill at a slower rate than expected [30,31,33,93]. Various proposals have been made to explain the observed reduction in the capillary filling rate of nanochannels, nevertheless the explanation is still under debate [30,33,93–96]. Since the interactions between the molecules present in the interface of the solid surface play a significant role on nanoscale capillary processes [8,35], we believe the presence of a gas layer at the silica–water interface, as inferred in our simulations, can influence the dynamic wetting [92] and thus affecting the capillary filling process in a silica nanochannel. Furthermore, a recent experimental study showed that water flow enhancement and slippage occurred in a hydrophilic nano channel [57], we believe that a plausible explanation could be related to the existence of air at the solid–liquid interface as reported in this study. In addition this layer of high density air at the interface may be the origin of nanobubbles as proposed in the experiments conducted by Zhang et al. [42,53].

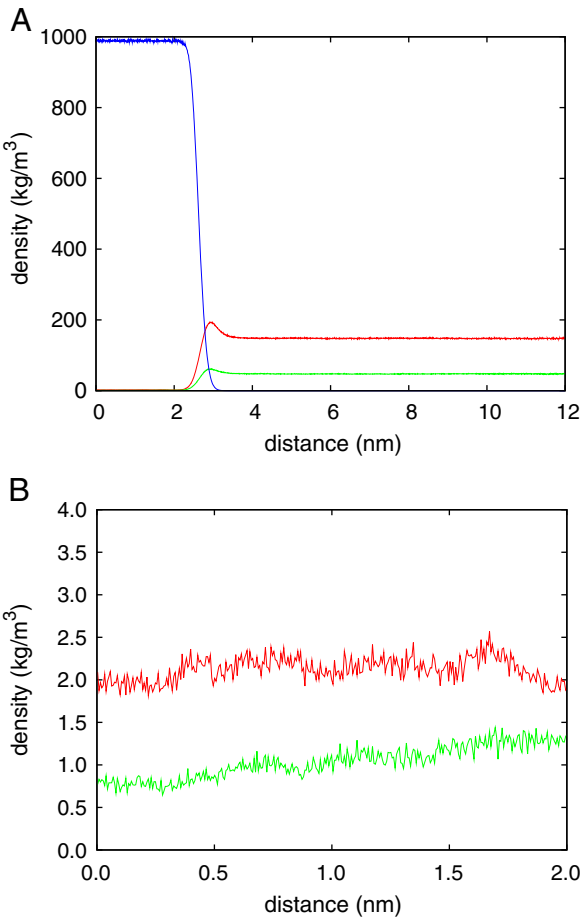

Fig. 5. Density of nitrogen and oxygen at 300 K and 200 bar in liquid water as a function of the distance to the center of mass of the water slab. (A) Density profiles of water, nitrogen and oxygen. The blue line is the water density profile, the red line is the N_2 density profile, and the green line is the O_2 density profile. (B) Details of the density profiles of nitrogen and oxygen dissolved in liquid water. The red line is the N_2 density profile, and the green line is the O_2 density profile.

Table 7
Calibrated Lennard–Jones parameters for the water–air interaction.

Parameter	Value
ϵ_{N-Ow}	0.5458 kJ mol^{-1}
σ_{N-Ow}	0.3243 nm
ϵ_{O-Ow}	0.5884 kJ mol^{-1}
σ_{O-Ow}	0.3078 nm

Table 8
Solubility of nitrogen and oxygen in liquid water computed from the MD simulations using the calibrated interaction potentials shown in Table 7.

Specie	Pressure	Solubility
N_2	100 bar	0.70 ± 0.34 cm$^3_{gas}$/g$_{H_2O}$
O_2	100 bar	2.72 ± 0.77 cm$^3_{gas}$/g$_{H_2O}$
N_2	200 bar	2.10 ± 0.62 cm$^3_{gas}$/g$_{H_2O}$
O_2	200 bar	3.54 ± 1.14 cm$^3_{gas}$/g$_{H_2O}$

Table 9
Water contact angle of water nanodroplets on a silica surface at different air pressures.

Pressure	Water contact angle
Vacuum	20°
50 bar	20°
100 bar	17°
150 bar	21°

Table 10
Silica–water binding energy at different air pressures.

Pressure	Binding energy
Vacuum	209 kJ mol^{-1} nm^{-2}
50 bar	226 kJ mol^{-1} nm^{-2}
100 bar	212 kJ mol^{-1} nm^{-2}
200 bar	222 kJ mol^{-1} nm^{-2}
300 bar	212 kJ mol^{-1} nm^{-2}

4. Conclusions

We have parameterized and calibrated an "effective" MD force field which is suitable for simulating nanofluidic phenomena in silica–water–air systems. We have conducted simulations of water nanodroplets on silica surfaces at different air pressures in order to study the role of the air on the water contact angle. Moreover, we have conducted MD simulations of bulk water on a silica substrate to investigate the silica–water interface in presence of air at different pressures. Adjacent to the immersed silica surface we observe a layer ca. 1 nm thick with high concentration of air. We hypothesize that this gas layer could be responsible for the unusual phenomena observed in experiments related to capillary filling of nanochannels observed experimentally. Furthermore, we believe that this layer with high density of gas could promote the nucleation of nanobubbles and influence its stability on a silica surface.

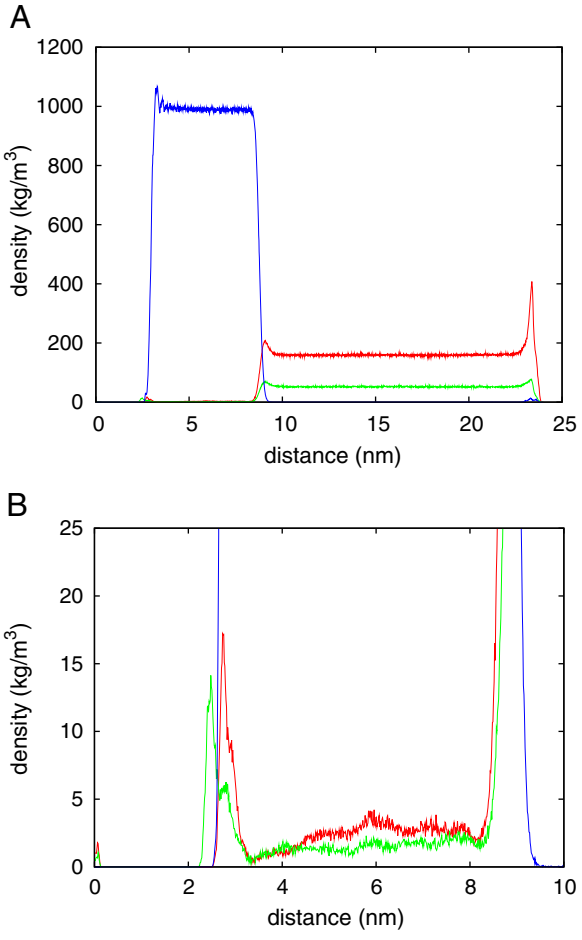

Fig. 6. Water slab on a silica substrate surrounded by air. Density profiles of water and air at 300 K and 200 bar. (A) Density profiles for the bulk zone of the system. (B) Details of the density profiles of air dissolved inside the water slab. The red line is the N_2 density, the green line is the O_2 density, and the blue line is the water density. The silica surface is located at ca. 2.7 nm, and it includes geometrical heterogeneities (molecular roughness).

Acknowledgment

Support for this work is provided in part by the Danish Research Council (grant no. 274-06-0465), and the Myhrwold, and Otto Mønsted Foundations. The authors wish to acknowledge discussion with Petros Koumoutsakos and computational support from the Danish Center for Scientific Computing (DCSC).

This research was presented at the 5th International Conference "Physics of Liquid Matter: Modern Problems" (Kyiv, Ukraine, 2010), http://www.plmmp.org.ua.

References

[1] L. Zhang, X. Zhang, Y. Zhang, J. Hu, H. Fang, Soft Matter 6 (2010) 4515–4519.
[2] J.L. Parker, P.M. Claesson, P. Attard, J. Phys. Chem. 98 (1994) 8468–8480.
[3] W.A. Ducker, Z. Xu, J.N. Israelachvili, Langmuir 10 (1994) 3279–3289.
[4] C. Huh, L.E. Scriven, J. Colloid Interface Sci. 35 (1971) 85–101.
[5] R.G. Cox, J. Fluid Mech. 168 (1986) 169–194.
[6] G. Saville, J. Chem. Soc. Faraday Trans. 5 (1977) 1122–1132.
[7] S. Romero-Vargas, N. Giovambattista, I.A. Aksay, P.G. Debenedetti, J. Phys. Chem. B 113 (2009) 1438–1446.
[8] J. DeConinck, T.D. Blake, Annu. Rev. Mater. Res. 38 (2008) 1–22.
[9] T.D. Blake, J. De Coninck, Adv. Colloid Interf. Sci. 96 (2002) 21–36.
[10] N. Giovambattista, P.G. Debenedetti, P. Rossky, J. Phys. Chem. B 111 (2007) 9581–9587.
[11] P. Abgrall, N.T. Nguyen, Anal. Chem. 80 (2008) 2326–2341.
[12] J. Ralston, M. Popescu, R. Sedev, Annu. Rev. Mater. Res. 38 (2008) 23–43.
[13] S. Villette, M.P. Valignat, A.M. Cazabat, L. Jullien, F. Tiberg, Langmuir 12 (1996) 825–830.
[14] S. Stavis, E.A. Strychalski, M. Gaitan, Nanotechnology 20 (2009) 165302.
[15] A. Ziemys, M. Ferrari, C. Cavasotto, J. Nanosci. Nanotechnol. 9 (2009) 6349–6359.
[16] L. Bocquet, E. Charlaix, Chem. Soc. Rev. 39 (2010) 1073–1095.
[17] J. Harrison, K. Fluri, K., S., Z. Fan, C. Effenhauser, A. Manz, Science 261 (1993) 895–897.
[18] M. Heller, Annu. Rev. Biomed. Eng. 4 (2002) 129–153.
[19] N. Douville, D. Huh, S. Takayama, Anal. Bioanal. Chem. 391 (2008) 2395–2409.
[20] J.K. Singh, Microfluid. Microfab. (2010) 309–331.
[21] L.T. Zhuravlev, Colloids Surf. A 173 (2000) 1–38.
[22] R.N. Lamb, D.N. Furlong, J. Chem. Soc. Faraday Trans. I 78 (1982) 61–73.
[23] M.-H. Du, A. Kolchin, H.-P. Cheng, J. Chem. Phys. 119 (2003) 6418–6422.
[24] W.A. Ducker, T. Senden, R.M. Pashley, Langmuir 8 (1992) 1831–1836.
[25] A.A. Hassanali, S.J. Singer, J. Phys. Chem. B 111 (2007) 11181–11193.
[26] B.P. Feuston, S.H. Garofalini, J. Appl. Phys. 68 (1990) 4830–4836.
[27] R. Thomas, F. Kaufman, J. Kirleis, R. Belsky, J. Electroanal. Chem. 143 (1996) 643–648.
[28] M. Nedyalkov, L. Alexandrova, Colloid Polym. Sci. 285 (2007) 1713–1717.
[29] E.R. Cruz-Chu, A. Aksimentiev, K. Schulten, J. Phys. Chem. B 110 (2006) 21497–21508.
[30] J.M. Oh, T. Faez, S. de Beer, Microfluid. Nanofluid. 9 (2010) 123–129.
[31] F. Persson, L.H. Thamdrup, M.B.L. Mikkelsen, S.E. Jaarlgard, P. Skafte-Pedersen, H. Bruus, A. Kristensen, Nanotechnology 18 (2007) 245301.
[32] L.H. Thamdrup, F. Persson, H. Bruus, A. Kristensen, H. Flyvbjerg, Appl. Phys. Lett. 91 (2007) 163505.
[33] N.R. Tas, J. Haneveld, H.V. Jansen, M. Elwenspoek, A. van den Berg, Appl. Phys. Lett. 85 (2004) 3274–3276.
[34] G. Martic, F. Gentner, D. Seveno, D. Coulon, J. De Coninck, T.D. Blake, Langmuir 18 (2002) 7971–7976.
[35] V.N. Phan, N.-T. Nguyen, C. Yang, P. Joseph, D. Bourrier, A.-M. Gue, Langmuir 26 (2010) 13251–13255.
[36] J.N. Israelachvili, R.M. Pashley, J. Colloid Interface Sci. 98 (1984) 500–514.
[37] P. Attard, J. Phys. Chem. 93 (1989) 6441–6444.
[38] N. Ishida, T. Inoue, M. Miyahara, K. Higashitani, Langmuir 16 (2000) 6377–6380.
[39] T.R. Jensen, M.Ø. Jensen, N. Reitzel, K. Balashev, G.H. Peters, K. Kjaer, T. Bjørnholm, Phys. Rev. Lett. 90 (2003) (086101).
[40] P. Ball, Nature 423 (2003) 25–26.
[41] B.M. Borkent, S.M. Dammer, H. Schonherr, G.J. Vancso, D. Lohse, Phys. Rev. Lett. 98 (2007) 204502.

[42] X.H. Zhang, X.D. Zhang, S.T. Lou, Z.X. Zhang, J.L. Sun, J. Hu, Langmuir 20 (2004) 3813–3815.
[43] X.H. Zhang, A. Khan, W.A. Ducker, Phys. Rev. Lett. 98 (2007) 136101.
[44] Y. Nam, S. Ju, Appl. Phys. Lett. 93 (2008) 103115.
[45] M.P. Brenner, D. Lohse, Phys. Rev. Lett. 101 (2008) 214505.
[46] A.P. Serro, R. Colaco, B. Saramago, J. Colloid Interface Sci. 325 (2008) 573–579.
[47] S.-T. Lou, Z.-Q. Ouyang, Y. Zhang, X.-J. Li, J. Hu, M.-Q. Li, F.-J. Yang, J. Vac. Sci. Technol. B 18 (2000) 2573–2575.
[48] R.E. Cavicchi, C.T. Avedisian, Phys. Rev. Lett. 98 (2007) 124501.
[49] P.S. Epstein, M.S. Plesset, J. Chem. Phys. 18 (1950) 1505–1509.
[50] S. Ljunggren, J.C. Eriksson, Colloids Surf. A 129 (1997) 151–155.
[51] C. Fradin, A. Braslau, D. Luzet, D. Smilgies, M. Alba, N. Boudet, K. Mecke, J. Daillant, Nature 403 (2000) 871–874.
[52] S. Mora, J. Daillant, K. Mecke, D. Luzet, A. Braslau, M. Alba, B. Struth, Phys. Rev. Lett. 90 (2003) 216101.
[53] X.H. Zhang, A. Quin, W.A. Ducker, Langmuir 24 (2008) 4756–4764.
[54] E. Dressaire, R. Bee, D.C. Bell, A. Lips, H.A. Stones, Science 320 (2008) 1198.
[55] W.A. Ducker, Langmuir 25 (2009) 8907–8910.
[56] J.H. Weijs, D. Lohse, Phys. Rev. Lett. 110 (2013) 054501.
[57] K.P. Lee, H. Leese, D. Mattia, Nanoscale 4 (2012) 2621–2627.
[58] J.H. Walther, R. Jaffe, T. Halicioglu, P. Koumoutsakos, J. Phys. Chem. B 105 (2001) 9980–9987.
[59] T. Werder, J.H. Walther, R. Jaffe, T. Halicioglu, F. Noca, P. Koumoutsakos, Nano Lett. 1 (2001) 697–702.
[60] J.H. Walther, T. Werder, R.L. Jaffe, P. Koumoutsakos, Phys. Rev. E. 69 (2004) 062201.
[61] J.H. Walther, T. Werder, R.L. Jaffe, P. Gonnet, M. Bergdorf, U. Zimmerli, P. Koumoutsakos, Phys. Chem. Chem. Phys. 6 (2004) 1988–1995.
[62] H.A. Zambrano, J.H. Walther, P. Koumoutsakos, I.F. Sbalzarini, Nano Lett. 9 (2009) 66–71.
[63] H.A. Zambrano, J.H. Walther, R.L. Jaffe, J. Chem. Phys. 131 (2009) 241104.
[64] R.L. Jaffe, P. Gonnet, T. Werder, J.H. Walther, P. Koumoutsakos, Mol. Simul. 30 (2004) 205–216.
[65] J.H. Walther, K. Ritos, E.R. Cruz-Chu, C.M. Megaridis, P. Koumoutsakos, Nano Lett. 13 (2013) 1910–1914.
[66] S. Tsuneyuki, M. Tsukada, H. Aoki, Y. Matsui, Phys. Rev. Lett. 61 (1988) 869–874.
[67] H.J.C. Berendsen, J.R. Grigera, T.P. Straatsma, J. Phys. Chem. 91 (1987) 6269–6271.
[68] D.W. Brenner, Phys. Status Solidi B 217 (2000) 23–40.
[69] Y. Guissani, B. Guillot, J. Chem. Phys. 104 (1996) 7633–7644.
[70] N.T. Huff, E. Demiralp, T. Cagin, W.A. Goddard III, J. Non-Cryst. Solids 253 (1999) 133–142.
[71] H.J.C. Berendsen, J.P.M. Postma, W.F. van Gunsteren, A. DiNola, J.R. Haak, J. Chem. Phys. 81 (1984) 3684–3690.
[72] M. Levitt, M. Hirshberg, K.E. Laidig, V. Daggett, J. Phys. Chem. B 101 (1997) 5051–5061.
[73] D.A.C. Beck, R.S. Armen, V. Daggett, Biochemistry 44 (2005) 609–616.
[74] J.N. Glosli, M.R. Philpott, J. Chem. Phys. 96 (1992) 6962–6969.
[75] I. Benjamin, J. Electroanal. Chem. 650 (2010) 41–46.
[76] E. Fadrna, K. Hladeckova, J. Koca, J. Biomol. Struct. Dyn. 23 (2005) 151–162.
[77] F.H. Song, B.Q. Li, C. Liu, Langmuir 29 (2013) 4266–4274.
[78] H.A. Zambrano, M. Pinti, A.T. Conlisk, S. Prasksh, Microfluid. Nanofluid. 13 (2012) 735–747.
[79] P. Angelikopoulos, C. Papadimitriou, P. Koumoutsakos, J. Phys. Chem. B 117 (2013) 14808–14816.
[80] J.-P. Ryckaert, G. Ciccotti, H.J.C. Berendsen, J. Comput. Phys. 23 (1977) 327–341.
[81] J. Jiang, J. Klauda, S. Sandler, J. Phys. Chem. B 108 (2004) 9852–9860.
[82] B.W.H. van Beest, G.J. Kramer, R.A. van Santen, Phys. Rev. Lett. 64 (1990) 1955–1958.
[83] A. Takada, P. Richet, C.R.A. Catlow, G.D. Price, J. Non-Cryst. Solids 345&346 (2004) 224–229.
[84] T. Werder, J.H. Walther, R.L. Jaffe, T. Halicioglu, P. Koumoutsakos, J. Phys. Chem. B 107 (2003) 1345–1352.
[85] T. Ingebrigtsen, S. Toxvaerd, J. Phys. Chem. C 111 (2007) 8518–8523.
[86] M.H. Du, L.L. Wang, A. Kolchin, H.P. Cheng, Eur. Phys. J. D 24 (2003) 323–326.
[87] A.K. Rappé, C.J. Casewit, K.S. Colwell, W.A. Goddard III, W.M. Skiff, J. Am. Chem. Soc. 114 (1992) 10024–10035.
[88] K.P. Travis, K.E. Gubbins, J. Chem. Phys. 112 (2000) 1984–1994.
[89] B. Coasne, A. Galarneau, F. DiRenzo, R.J. Pellenq, Langmuir 26 (2010) 10872–10881.
[90] R. Wiebe, V.L. Gaddy, C. Heins, J. Am. Chem. Soc. 55 (1933) 947–953.
[91] V.I. Baranenko, L.N. Fal'kovskii, V.S. Kirov, L.N. Kurnyk, A.N. Musienko, A.I. Pointkovskii, Sov. J. At. Energy 68 (1990) 342–346.
[92] G. Nagayama, P. Cheng, Int. J. Heat Mass Transfer 47 (2004) 501–513.
[93] J. Haneveld, N. Tas, N. Brunets, H. Jansen, M. Elwenspoek, J. Appl. Phys. 104 (2008) 014309.
[94] J. van Honschoten, N. Brunets, N.R. Tas, Chem. Soc. Rev. 39 (2010) 1096–1114.
[95] V.D. Sobolev, N.V. Churaev, M.G. Velarde, Z.M. Zorin, Colloid J. 63 (2001) 127–131.
[96] N.A. Mortensen, A. Kristensen, Appl. Phys. Lett. 92 (2008) 063110.